Pu Huang [1,*] Zhiguo Xia [2,*,†] Xiaoqing Gao,[1] James M. Rondinelli,[3] Xiuwen Zhang [1,‡] Han Zhang,[4]
Kenneth R. Poeppelmeier [5,§] and Alex Zunger [6,]
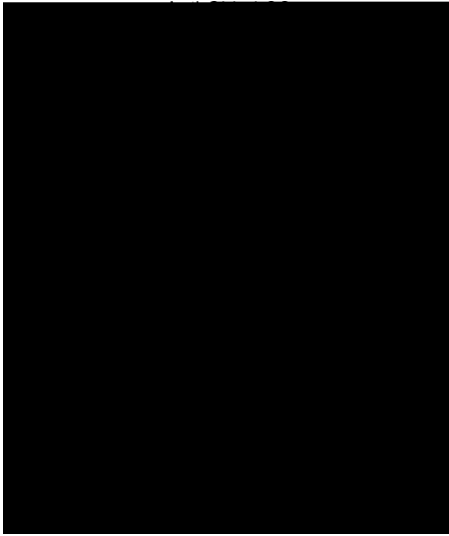
1

FIG. 1. Schematic depiction of how achiral centrosymmetric (CS) symmetry can decompose into two ferri-chiral (FEC) structures FEC-1 and FEC-2 that are Non-CS. The special case discussed here occurs when the FEC structures exhibit the Dresselhaus effect D-1_B, where at least one site has polar symmetry. This behavior is distinct from the standard Dresselhaus effect D-1_A where all sites are nonpolar, as in the zinc-blende structure.

Zhang   . noted [1] that the definition of different bulk spin-splitting functionalities determined by the point-group and space-group symmetries depends on additional aspects of the site symmetries of the individual Wyckoff positions occupied by the atoms in the structure. Although the Dresselhaus effect requires a nonpolar Non-CS crystal class for the space group [6], it can be further differentiated into three subclasses based on the occupied site symmetries in the crystal [1]. In the traditional D-1_A effect each occupied site must be nonpolar, whereas in D-1_B at least one site must be polar, however, the net electric polarization must be zero, i.e., the sum of dipoles arising from local displacements is zero. In contrast, D-1_C polar sites must be occupied, but the sum of dipoles is nonzero. Herein we focus on the D-1_B effect, which although similar to the Rashba effect differs in that there is zero net electric polarization. Chiral crystals with polar individual site symmetries (e.g., LiAlO$_2$) are examples of D-1_B materials which compensate each other even though they are not inversion partners. This special Dresselhaus spin splitting enabled by crystallographic chirality is rarely studied but could also be used to remove the Kramer's degeneracy in crystals with relativistic interactions and access spin-polarized carriers in nonmagnetic compounds.

Here we focus on ferri-chiral materials, where two sets of chiral units differentiated by opposite distortion senses cannot exactly compensate each other (Fig. 1). The direction of these small atomic displacements governs the spin-split electronic band structure, which can be reversed upon changing the orientations of these units. We identify NaCu$_5$S$_3$ as a stable ferri-chiral compound by symmetry screening in the diverse family of alkali metal copper chalcogenides followed by analysis of the spin splitting in the electronic structure with density functional calculations. We then synthesize NaCu$_5$S$_3$ and computationally demonstrate that the Dresselhaus spin splitting is interlocked with its ferri-chirality. We show that application of modest strain significantly reduces the barrier between the two orientations of ferri-chiral NaCu$_5$S$_3$ [. . .]
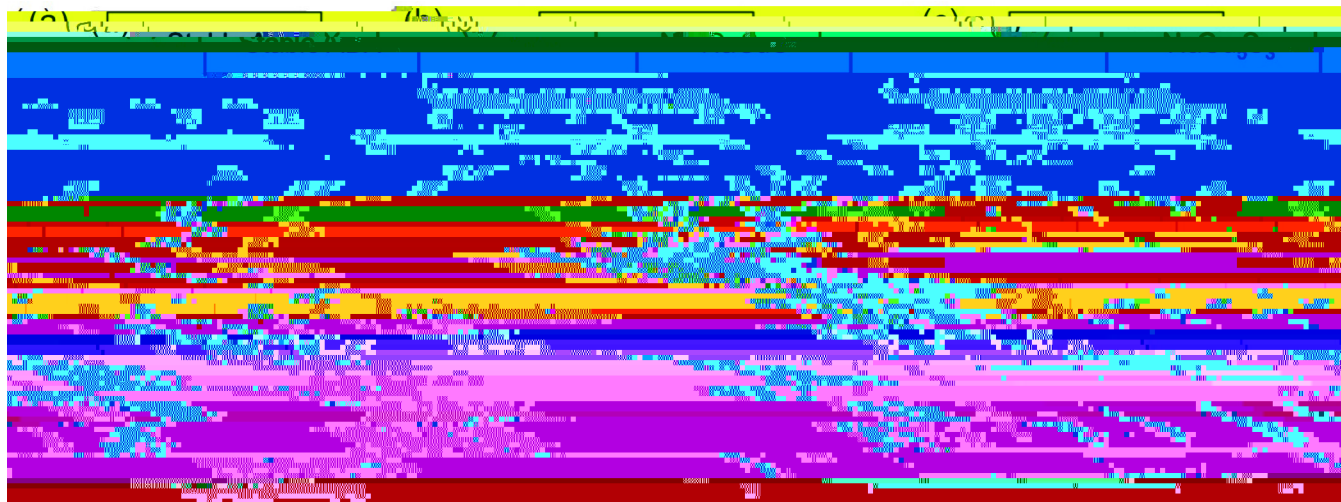
FIG. 2. Stability assessment of alkali metal copper chalcogenides. (a) Predicted (+ signs) and previously reported (check marks) I-I-VI compounds. (b), (c) Stability regions (green zones) of NaCuS and NaCu

FIG. 8. (a) Partial density of states (PDOS) for $NaCu_5S_3$ with 6_322 (FEC-1/2) and $6_3/$ (AC) symmetries from DFT + U ($U = 6$ eV) without SOC. (b) Charge densities ($\varepsilon = 0.02$ Å^{-3}) of the FEC-1/2 and AC phases.

displacements of Cu-1 in the CuS_2 chain [Fig. 3(d)] and Cu-2 (in the CuS_3 triangle) that transform as the irreducible representation Γ_1^-. Although CuS_2 linear chains have been found in copper chalcogenides [11], CuS_3 planar triangles are an uncommon coordination for copper, which provides a driving force for bond distortion to a nonplanar structure as follows: Cu-1 displaces within the plane, which removes one mirror plane, whereas Cu-2 displaces along the axis, eliminating the reflection operation perpendicular to the sixfold axis. Chirality arises in this structure because of a perceptual rotation sense due to the antisymmetric displacements on the copper planes, as illustrated for the ferri-chiral phase of $NaCu_5S_3$ with red/blue arrows in Fig. 4(c), which together remove the glide operation. Indeed, these local 3-in-2-out (or 3-out-2-in) displacements exhibit dihedral symmetry; however, their combination results in partial instead of full compensation of the $^+$ and $^-$ chiralities to produce the ferri-chiral structures with 6_322 symmetry. The chiral motifs and the mechanism of ferri-chirality of NaCu
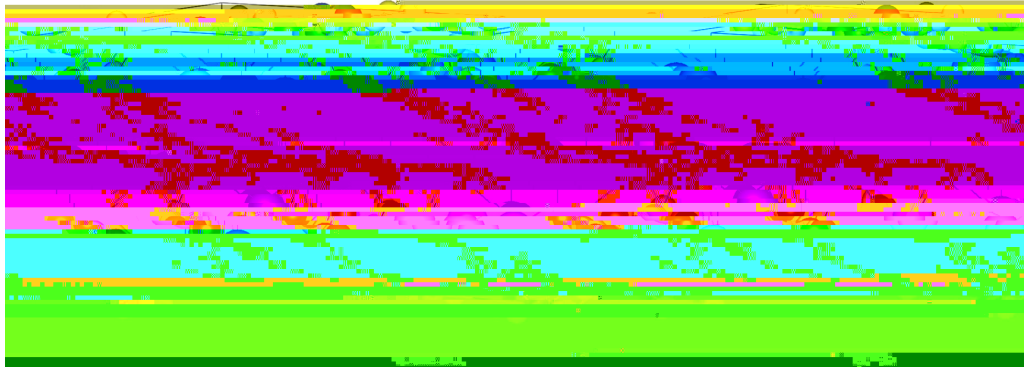
FIG. 10. Comparison for the partial charge densities (= 0.004 Å^{-3}) at the Γ point of the VBM obtained from DFT + (= 6 eV) and HSE06.

spin splitting (Fig. 6). Band structures and electronic densities of states (along with charge densities) obtained without SOC are shown in Figs. 7 and 8, respectively, of Appendix C. Figure 9 compares the band dispersions without SOC obtained using a screened hybrid functional (HSE06 [23,24]) against our DFT + results, showing good agreement between the two levels of theory. Figure 10 shows that the partial charge densities at the Γ point of the valence-band maximum (VBM) evaluated with DFT + and HSE06 approaches are also in good agreement. Figure 11 shows the effect of different choices of on the band structure without SOC. Both the spin-splitting magnitude and the linear spin-splitting coefficient are weakly dependent on the Hubbard used for Cu. The valence-band spin-splitting energy and spin-splitting coefficient are 194/208 meV and 261/275 meV Å for pristine $NaCu_5S_3$ with = 0/6 eV, respectively.

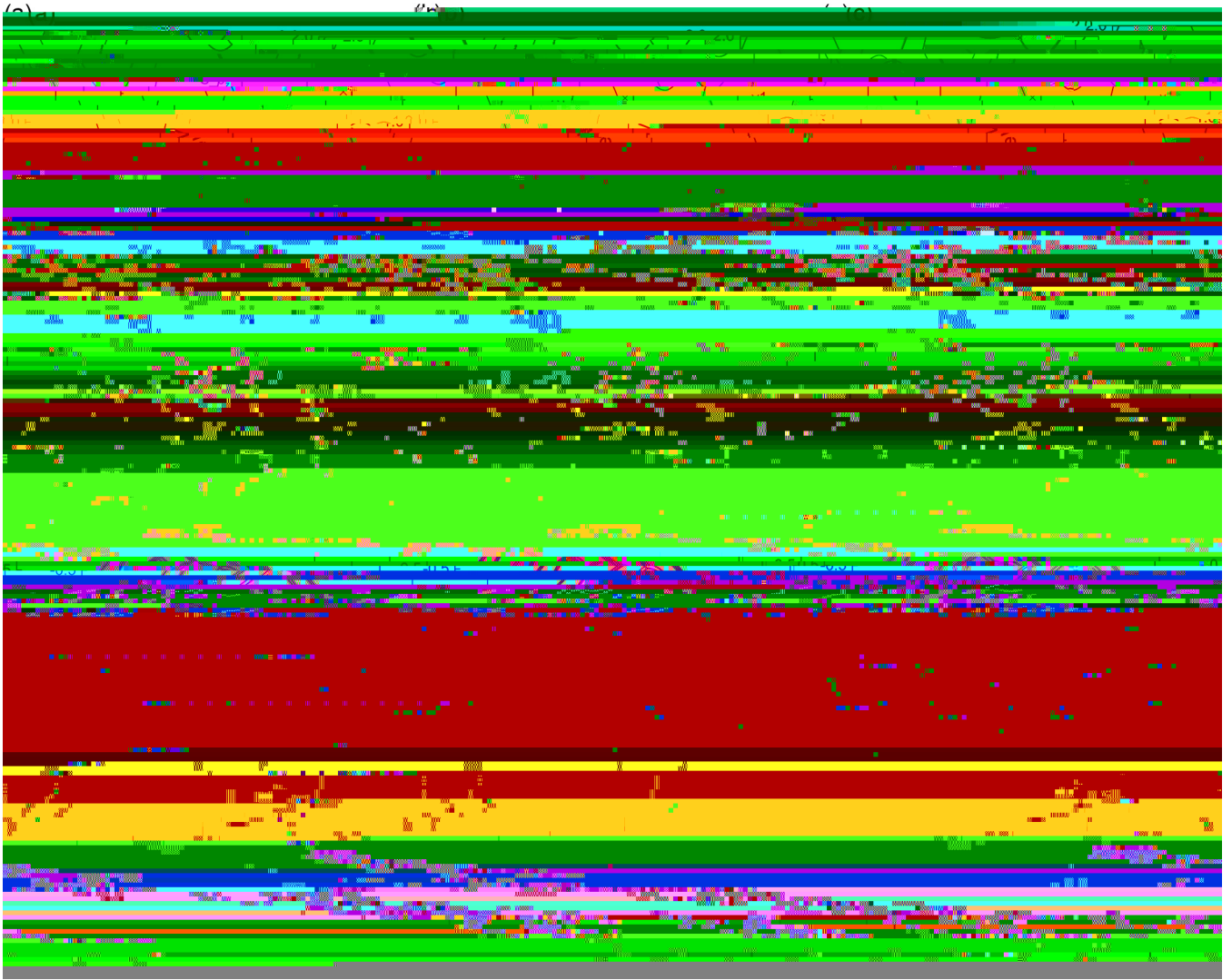Detailed band structures near the VBM in Figs. 6(c)–6(e)

FIG. 12. Atomic and orbital projected band structures (a)–(h) of NaCu$_5$S$_3$ with 6$_3$
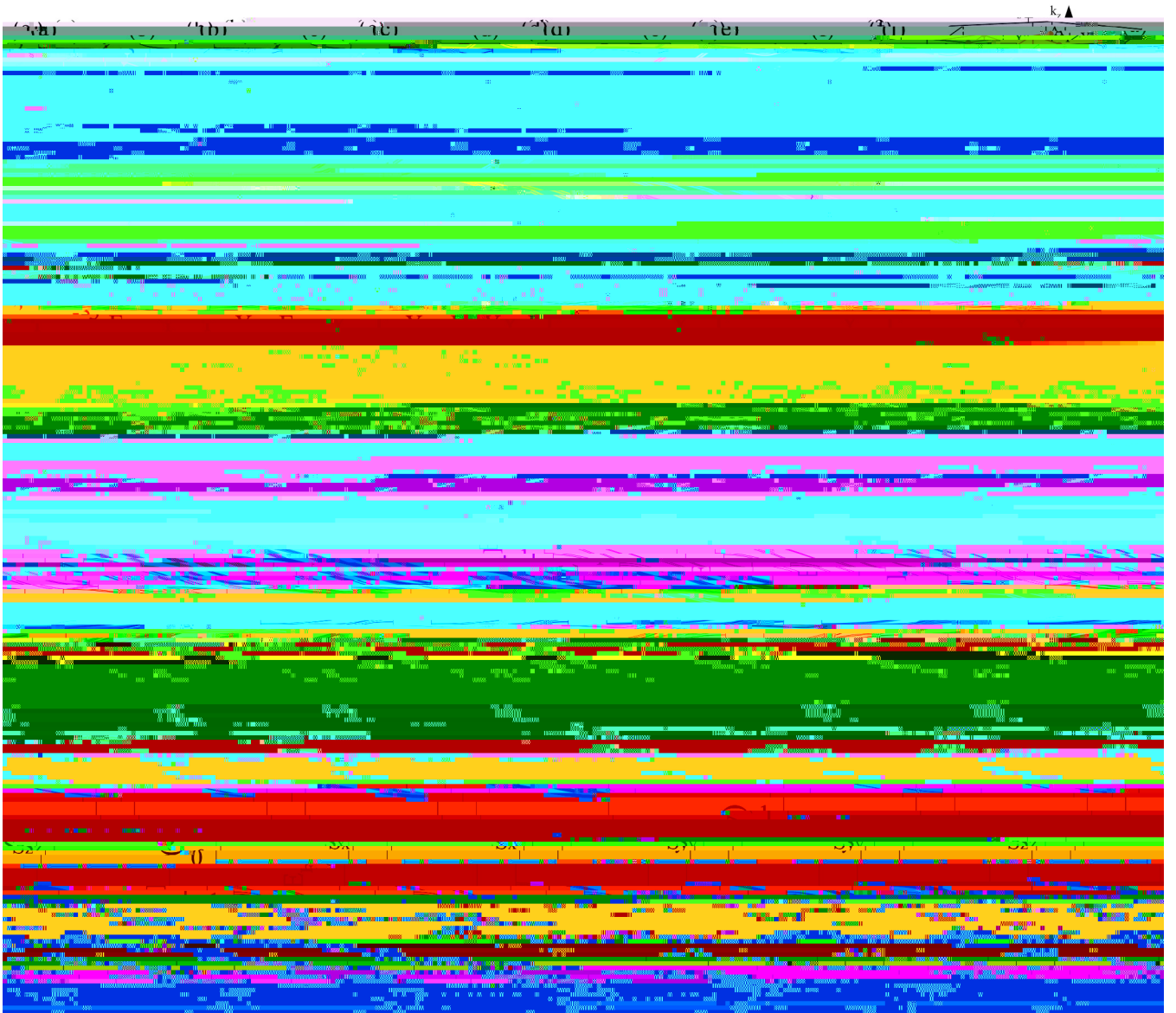
FIG. 16. Spin components of the energy bands in the FEC-1 structure of NaCu$_5$S$_3$ along $\Gamma-$, $B-$, and $A-$ paths. Inset: Brillouin zone of NaCu$_5$S$_3$ illustrating the $\Gamma-$, $B-$, and $A-$ paths.

displacements that break the full compensation of $^+$ and $^-$ chiralities can be restored [see the variation of the crystallographic parameters in Fig. 17(b)] and the CS antichiral phase ($6_3/$) is stabilized as the ferri-chiral transition barrier is quenched. Figure 5
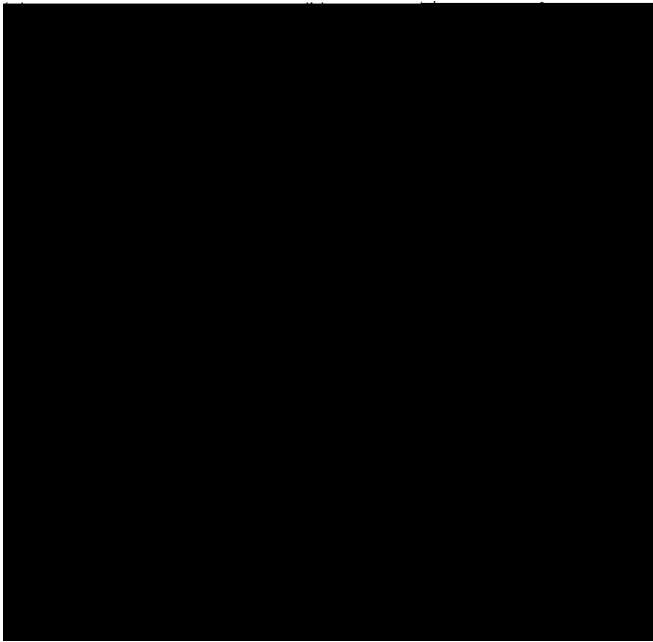
FIG. 17. Tunable ferri-chiral phase transition and spin splitting in $NaCu_5S_3$. (a) Transition barrier between the two ferri-chiral phases of $NaCu_5S_3$. The black dashed curve corresponds to the unstrained case, and other curves correspond to different strain values. (b) Detailed crystallographic information including the movement of Cu-2 away from the center of the CuS_3 planar triangle along [001] lattice direction (Δ), the movement of Cu-1 away from the center of the CuS_2 linear chain as represented by the S-Cu-S angle ( ), and along the transition between FEC-1/2 and AC states under external biaxial strain in the   plane. The $+/-$ signs represent tensile and compressive strain. (c), (d) Low-energy valence bands in the $\Gamma - A$ direction for the FEC-1 ferri-chiral phase of $NaCu_5S_3$ under uniaxial strain along the   lattice direction. Red/blue colors indicate the spin projection, with the spin polarization axis along the   direction. The gray background indicates the magnitude of the spin-splitting energy. Similar tunability of spin-splitting energy under   / uniaxial/biaxial strains is demonstrated in Fig. 18, in the Appendixes.

. ✔ N ●Ĺ   N

In summary, we designed a type of ferri-chiral material with potentially switchable Dresselhaus spin splitting via a combined theoretical and experimental study. The nonconventional Dresselhaus effect D-1$_B$